996 *Biochemistry* **2010,** *49,* 996–1004
DOI: 10.1021/bi901339n

BIOCHEMISTRY
including biophysical chemistry & molecular biology
*Article*

# Kinetic and CD/MCD Spectroscopic Studies of the Atypical, Three-His-Ligated, Non-Heme $Fe^{2+}$ Center in Diketone Dioxygenase: The Role of Hydrophilic Outer Shell Residues in Catalysis†

Grit D. Straganz,*[,‡,§] Adrienne R. Diebold,[§] Sigrid Egger,[‡] Bernd Nidetzky,[‡] and Edward I. Solomon[§]

[‡]*Institute of Biotechnology and Biochemical Engineering, Graz University of Technology, Petersgasse 12, A-8010 Graz, Austria and* [§]*Department of Chemistry, Stanford University, Stanford, California 94305*

*Received August 3, 2009; Revised Manuscript Received January 4, 2010*

ABSTRACT: Diketone cleaving enzyme (Dke1) is a dioxygenase with an atypical, three-histidine-ligated, mononuclear non-heme $Fe^{2+}$ center. To assess the role in enzyme catalysis of the hydrophilic residues in the active site pocket, residues Glu98, Arg80, Tyr70, and Thr107 were subjected to mutational analysis. Steady state and pre-steady state kinetics indicated a role for Glu98 in promoting both substrate binding and $O_2$ reduction. Additionally, the Glu98 substitution eliminated the pH dependence of substrate binding ($k_{cat}^{app}/K_M^{app}$−pH profile) present in wild-type Dke1 ($pK_a = 6.3 \pm 0.4$ and $8.4 \pm 0.4$). MCD spectroscopy revealed that the Glu98 → Gln mutation leads to the conversion of the six-coordinate (6C) resting $Fe^{2+}$ center present in the wild-type enzyme at pH 7.0 to a mixture of five-coordinate (5C) and 6C sites. The 6C geometry was restored with a pH shift to 9.5 which also resulted in ligand field (LF) energy splittings identical to that found for wild-type (WT) Dke1 at pH 9.5. In WT Dke1, these LF transitions are shifted up in energy by ∼300 $cm^{-1}$ at pH 9.5 relative to pH 7.0. These data, combined with CD pH titrations which reveal a $pK_a$ of ∼8.2 for resting WT Dke1 and the Glu98 → Gln variant, indicate the deprotonation of a metal-ligated water. Together, the kinetic and spectroscopic data reveal a stabilizing effect of Glu98 on the 6C geometry of the metal center, priming it for substrate ligation. Arg80 and Tyr70 are shown to promote $O_2$ reduction, while Thr107 stabilizes the Fe(II) cofactor.

Mononuclear non-heme $Fe^{2+}$ centers are important for the catalysis of a variety of highly specific $O_2$-dependent reactions (*1*−*3*). A common rationale is often employed in these enzymes: a facial triad of two histidines and one glutamate/aspartate together with two or three water molecules ligate the resting $Fe^{2+}$ cofactor. In the presence of all reaction components, a catalytically competent five-coordinate (5C)[1] metal center is formed, which allows $O_2$ binding and reduction, coupled with substrate oxidation (*3*). The facial triad is considered to play various roles, including (i) creating a high-affinity $Fe^{2+}$ binding site, (ii) providing a geometric scaffold that allows coordination of $O_2$ to the $Fe^{2+}$ center upon cosubstrate and/or substrate binding to the enzyme, and (iii) maintaining the appropriate redox potential of the metal center.

The facial triad is embedded in the protein environment, which typically affords selective binding and appropriate positioning of the substrate and, if required, cosubstrate. The active site pocket may also provide proteinogenic residues that promote reaction steps via acid−base catalysis or H-bonding interactions. In the reaction mechanism of extradiol catechol ring-cleaving dioxygenases, results from detailed pre-steady state and steady state kinetic, mutational, and computational studies have demonstrated roles for specific hydrophilic active site residues in substrate binding, $O_2$ reduction, and C−C bond cleavage (*4*−*7*). Additionally, the H-bonding network in the active site will contribute to the de/stabilization of outer and inner shell water which can participate in catalysis. Metal-bound waters, furthermore, directly determine the metal center coordination number and, consequently, cofactor stability and the catalytic competence of the metal center. While a 6C metal center is believed to protect $Fe^{2+}$ from uncoupled oxidation by $O_2$ when only cofactor is present, formation of a 5C center upon ligation of all (co)substrates is required for efficient catalysis. The facial triad itself has been shown to contribute directly to the H-bonding network of non-heme iron enzymes. In the α-ketoglutarate-dependent dioxygenases, the carboxylate ligand of the facial triad plays a role in stabilizing water coordination through a H-bonding interaction between the noncoordinating oxygen of the carboxylate and the coordinated water (*8*).

In recent years, a small number of $O_2$-dependent non-heme iron enzymes have been found that exhibit distinct metal binding motifs (*9*). The rationale for these deviations and the resulting consequences are under active investigation. In the case of the α-ketoglutarate- and $O_2$-dependent halogenases SyrB2 (*10*) and CytC3 (*11*), the natural substitution of the metal ligating carboxylate of the facial triad with alanine leaves space for a halide ion, which is the substrate in the halogenation reaction. This mechanistically driven

†G.D.S. gratefully acknowledges funding of this work by the FWF (Austrian Science Fund, Project P18828) and support of the joint work by the Max Kade Foundation. E.I.S. acknowledges National Institutes of Health Grant GM 40392 for support.

*To whom correspondence should be addressed: Institute of Biotechnology and Biochemical Engineering, Graz University of Technology, Petersgasse 12, A-8010 Graz, Austria. E-mail: grit.straganz@tugraz.at. Telephone: +43-316-873-8414. Fax: +43-316-873-8434.

[1]Abbreviations: Dke1, diketone cleaving enzyme; 4C, 5C, and 6C, four-, five-, and six-coordinate, respectively; LF, ligand field; CD, circular dichroism; MCD, magnetic circular dichroism; PDB, Protein Data Bank; QSAR, quantitative structure−activity relationship; PD, 2,4-pentanedione; TFPD, 1,1,1-trifluoro-PD; DFPB, 4,4-difluoro-1-phenyl-1,3-butanedione; TFPB, 4,4,4-trifluoro-1-phenyl-1,3-butanedione; PB, phenyl-1,3-butanedione; DFPD, 1,1-difluoro-2,4-pentanedione; WT, wild type.

 Published on Web 01/05/2010 

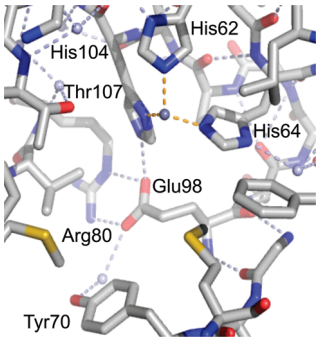


FIGURE 1: Metallocenter and H-bonding network in Dke1, the primary enzyme of the acetylacetone degradation pathway in *A. johnsonii* [PDB entry 3bal (*12*)]. First-sphere histidines and hydrophilic active site residues are labeled accordingly. Note the structure is for the Zn-substituted form, and no $H_2O$ was resolved. Carbons, oxygens, nitrogens, and sulfurs are colored gray, red, blue, and yellow, respectively. H-Bonds are colored blue.

deviation from the facial triad motif comes at the cost of losing a high-affinity $Fe^{2+}$ binding site in the resting enzyme.

In the C−C bond cleaving dioxygenase Dke1, which displays a high-affinity three-His $Fe^{2+}$ binding site [Figure 1; PDB entry 3bal (*12*)], a clear rationale for this deviation in metal binding motif, which it shares only with cysteine dioxygenase, is still missing.[2] We have studied the role of the first coordination sphere of Dke1, which constitutes the primary enzyme of the acetylacetone degradation pathway in *Acinetobacter johnsonii* (*13*, *14*), in metal binding and catalysis. Spectroscopic investigations, employing a combination of near-infrared circular dichroism (CD), magnetic circular dichroism (MCD), and variable-temperature, variable-field MCD spectroscopies, have revealed that Dke1 follows the general mechanistic strategy of $O_2$ activation by the facial triad ligated $Fe^{2+}$ center, showing a 6C resting site and partial conversion to a 5C species upon substrate ligation (*15*). Mutation of the first coordination sphere to a facial triad leads to the destruction of the high-affinity metal binding site (*16*), preventing study of a restructured facial triad.

Here we report a detailed investigation of the role of the outer shell residues in the enzyme's structural stability and reactivity. Previous steady state and single-turnover enzyme kinetics together with quantitative structure−activity relationship (QSAR) studies have allowed dissection of particular steps of the chemical reaction and have implied a chemical mechanism (*17*, *18*). $O_2$ reduction is the rate-limiting step of the enzymatic reaction under physiological conditions, and $O_2$ reduction and C−O bond formation are concerted. In this study, these methods are combined with mutational and CD and MCD spectroscopic methods to gain detailed insight into the interplay of second-shell residues and the structure and function of the three-His metal center. Results reveal marked effects of particular outer shell residues on cofactor stability, active site geometry, substrate binding, and $O_2$ reduction rates. The roles of the respective amino acid residues in specific reaction steps are discussed.

## MATERIALS AND METHODS

*Materials*. 2,4-Pentanedione (PD), 1,1,1-trifluoro-PD (TFPD), 4,4-difluoro-1-phenyl-1,3-butanedione (DFPB), 4,4,4-trifluoro-1-phenyl-1,3-butanedione (TFPB), phenyl-1,3-butanedione (PB), and other chemicals were obtained from Sigma Aldrich (St. Louis, MO), except 1,1-difluoro-2,4-pentanedione (DFPD) which was from Matrix Scientific (Columbia, SC). All substrates were purchased at the highest available quality (>97% pure) if not otherwise stated. *Pfu* DNA polymerase was from Promega (Madison, WI). The other enzymes for molecular biology were purchased from MBI Fermentas (St. Leon-Rot, Germany). Expression vector pKYB1 was from New England Biolabs (Beverly, MA).

*Methods*. (*i*) *Site-Directed Mutagenesis and Enzyme Preparation*. Site-directed mutations were introduced via a standard two-stage PCR protocol (*19*). Two separate primer extension reactions were performed using the respective forward and reverse oligonucleotide primer (Table 1) and plasmid vector pKYB1-*dke1 Strep* (*20*) as a template. The latter contains the full-length *dke1* gene fused to an oligonucleotide encoding a 10-amino acid C-terminal affinity tag (*21*). Note that we have demonstrated, previously, that heterologous expression and the affinity tag do not alter the biochemical and catalytic properties of Dke1 (*20*), which we originally isolated from *A. johnsonii* (*13*, *14*). For the introduction of multiple mutations, the respective mutation-bearing analogous vector was used. The PCR protocol used 150 ng of template in a total volume of 25 μL. Four cycles of separate amplification with 3 units of *Pfu* DNA polymerase (Promega) were followed by 18 cycles of amplification of the combined reaction mixtures using an annealing temperature of 62 °C. The final extension phase was 15 min at 72 °C. After digestion of the template DNA with *Dpn*I, the amplified plasmid vectors were transformed into electro-competent *Escherichia coli* BL21(DE3) cells (Stratagene, La Jolla, CA) according to standard procedures. Plasmid DNA from positive clones was isolated via a miniprep kit (Wizard Plus SV Minipreps, Promega) and subjected to dideoxy sequencing of the entire *dke1* gene, to verify that the clone bore the desired mutation and that no errors had been introduced into the sequence during amplification via PCR.

Production of recombinant wild-type Dke1 and variants of Dke1 was done according to the procedures described previously (*20*). Purification was conducted according to reported protocols, using affinity chromatography with a 1 mL *Strep*-Tactin column (IBA, Goettingen, Germany) and subjected to buffer exchange by three passages of desalting via NAP-25 columns (GE Healthcare, Chalfont St. Giles, Great Britain) using 20 mM Tris-HCl buffer (pH 7.5). Protein solutions were concentrated (≥10 mg/mL, >95% pure) with Vivaspin centrifugation concentrator tubes (Vivascience, Hannover, Germany) and stored at −20 °C.

(*ii*) *$Fe^{2+}$ Content and Protein Concentration*. The content of protein-bound $Fe^{2+}$ in purified enzyme preparations was determined spectrophotometrically, whereby the formation of a colored solution complex between $Fe^{2+}$ and ferene S ($\varepsilon_{592} = 35.5$ $mM^{-1}$ $cm^{-1}$) (*22*, *23*) was monitored in an overnight measurement. All assays were performed at 25 °C in 20 mM Tris-HCl buffer (pH 7.5), containing ferene S in excess (20 mM) and 2 mM ascorbic acid as a reductant, to keep $Fe^{2+}$ in its reduced form over time. Blanks in the absence of protein were measured and subtracted. Protein concentrations were determined by measuring the absorbance at 280 nm of the appropriately diluted purified enzyme preparation in Tris buffer (20 mM, pH 7.5) and applying a theoretically calculated absorption coefficient from the respective sequence on the basis of the method of Edelhoch (*24*) and the parameters of Pace (*25*) using ProtParam (http://www.expasy.ch). Note that this method, which uses native

[2]Sequence alignments with cysteine dioxygenase suggest a three-His metal binding motif also for cysteamine- and 3-mercaptopropioate dioxygenase. Direct evidence from protein structures, however, is not available.

Table 1: Primers and Template DNA Used in This Study To Generate Dke1 Variants, with Mutations Underlined in the Primer Sequence

| Target-variant | Template:[a] | Primer (5'→3') |
|---|---|---|
| T107A | WT [b] | fw: *5'-CATTGCATGGTAAAGCTTTCTTTCCTGTCG-3'* |
| | | rev: *5'-CGACAGGAAAGAAAGCTTTACCATGCAATG-3'* |
| E98Q | WT | fw: *5'-CCAAGCTACGGTTTTCAGTCTTCAGGTGCATTGC-3'* |
| | | rev: *5'-GCAATGCACCTGAAGACTGAAAACCGTAGCTTGGTG-3'* |
| E98A | WT | fw: *5'-CCAAGCTACGGTTTTGCGTCTTCAGGTGCATTGC-3'* |
| | | rev: *5'-CAATGCACCTGAAGACGCAAAACCGTAGCTTGGTGC-3'* |
| R80A | WT | fw: *5'-GAAAAATGGAAGTGGCTGGTGGCGAGCAAG-3'* |
| E98A_R80A | E98A | rev: *5'-CTTGCTCGCCACCAGCCACTTCCATTTTTC-3'* |
| Y70F | WT | fw: *5'-CATGCTGGCCCCGGGGAATTTTTCCTGACTAAGGG-3'* |
| E98A_R80A_Y70F | E98A_R80A | rev: *5'-CCCTTAGTCAGGAAAAATTCCCCGGGGCCAGCATG-3'* |
| Y70A | WT | fw: *5'-CATGCTGGCCCCGGTGAAGCTTTCCTGACTAAGGGAAAA-3'* |
| E98A_R80A_Y70A | E98A_R80A | rev: *5'-CATTTTTCCCTTAGTCAGGAAAGCTTCACCGGGGCCAGCATG-3'* |

[a]The template was the pKYB1-*dke1 Strep* vector, bearing the respective, outlined mutation. [b]Wild-type plasmid.

protein, gave the same results as the standard procedure, which uses denaturing conditions [6 M guanidine·HCl buffer and 20 mM $KH_2PO_4/K_2HPO_4$ (pH 6.5)] within an experimental error of 5%. The method was furthermore validated using the BCA method (Pierce, Rockford, IL). Apparent first-order iron detachment rates were determined using Microcal Origin.

(*iii*) *Steady State Kinetics*. The standard assay of Dke1 activity was conducted at 25 °C using 0.2 mM PD dissolved in air-saturated 20 mM Tris-HCl buffer (pH 7.5). The rate of substrate depletion was measured spectrophotometrically at 280 nm and 25 °C with a DU 800 UV−vis spectrophotometer (Beckmann Coulter, Inc., Fullerton, CA).

Steady state kinetic studies with PD and TFPD at different pH values were performed in 100 mM MES (pH 5.0−6.5) and Tris (pH 6.5−10.5) buffer, whereby the absorbance trace at the wavelength of maximum substrate absorbance was monitored (*18*).[3] The pH dependence of extinction coefficients had been determined previously (*18*), and reaction rates were calculated accordingly. Specific activities and apparent $k_{cat}^{app}$ values were generally related to the concentration of $Fe^{2+}$-containing enzyme active sites, which were calculated from the iron content in the gel filtered protein preparation as described (vide supra).

$K_M^{app}$ and $k_{cat}^{app}$ values were obtained in two ways. (i) A series of classical initial rate measurements at varied substrate concentrations and a nonlinear fit of the Henri−Michaelis−Menten equation for a single-substrate enzymatic reaction to the data were performed. (ii) To validate initial rate data, the integrated form of the Michaelis−Menten equation to expanded reaction time courses was applied, whereby 50 $\mu$M substrate was used and rates were corrected for the decrease in $O_2$ concentration. It was shown that both approaches to kinetic analysis yielded consistent estimates for the apparent catalytic center activity ($k_{cat}^{app}$) and Michaelis−Menten constant ($K_M^{app}$) at 260 $\mu$M $O_2$, whereby the integrated approach allows for a better assessment of rates at low substrate concentrations.

[3]Given that Dke1 activity is insensitive to an increase in ionic strength, as tested at salt concentrations of up to 1 M NaCl, the change in ionic strength at various pH values was neglected.

(*iv*) *Substrate Binding Kinetics*. Formation of the enzyme−$Fe^{2+}$−substrate complex was assessed with a stopped-flow UV−vis spectrophotometer (SF61DX2, Hi-Tech) housed in an argon-flushed glovebox (Belle Technology), monitoring the prototypical low-energy transition of the substrate-ligated metal center at the wavelength of its maximum absorbance, $\lambda_{max}$ (*18*). Stock solutions of substrate (300 $\mu$M) and enzyme (300 $\mu$M $Fe^{2+}$, 600 $\mu$M enzyme subunits) were used, which had been made anaerobic by being repeatedly flushed with nitrogen. Note that the substrate concentration was fully saturating at the steady state ($K_M^{app} < 10\ \mu$M). The reaction was conducted at 25 °C in an air-saturated 20 mM Tris-HCl buffer (pH 7.5).

Binding kinetics showed biphasic behavior and were best fit via the following formula describing double-exponential decay:

$$A = a_0 - a_1 e^{-(k_1 t)} - a_{1'} e^{-(k_{1'} t)} \quad (1)$$

where $A$ is the absorbance, $a_0$ is the total amplitude, and $a_1$ and $a_{1'}$ are the amplitudes of the respective binding steps that proceed with first-order rate constants of $k_1$ and $k_{1'}$, respectively. All measurements were taken in triplicate, and resulting rate constants were averaged.

(*v*) *CD and MCD Spectroscopy*. Apoenzyme was prepared by dialyzing Dke1 against 20 mM EDTA in 20 mM Tris-HCl buffer (pH 7.5) at 4 °C for 2 days using a Slide-A-Lyzer cassette (Pierce), with repeated buffer exchange, and for an additional 2 days against the Tris buffer without EDTA. The resulting apoenzyme was then buffer exchanged into 100 mM Tris-HCl in $D_2O$ at the appropriate pD, using a 4 mL Amicon Ultra-4 filter with a 10 kDa cutoff membrane (Millipore), and the protein was then brought to a monomer concentration of ~1−2 mM. Reagents were made anaerobic by purging with argon gas on a Schlenk line. Dke1 was made anaerobic by alternating cycles of evacuation and argon purge on the Schlenk line at 0 °C. All samples were prepared under an inert atmosphere inside a $N_2$-purged "wet box" to maintain an $O_2$ free environment. Ferrous ammonia sulfate was added in microliter quantities to a final concentration of 90% of the monomer concentration. The samples were then transferred into an anaerobic cuvette and incubated for ~1 h in the glovebox, prior to measurement.

Saturating amounts of deuterated sucrose were added anaerobically to protein preparations as a glassing agent for MCD measurements to a final concentration of ~1 mM active sites. CD measurements were taken without and with sucrose to ensure that the $Fe^{2+}$ site was unaffected by the glassing agent. (Note that sucrose, rather than glycerol, was used as a glassing agent as the latter affected the NIR CD spectrum of the $Fe^{2+}$ active site.)

Near-IR (600−2000 nm) CD and MCD data were recorded on a Jasco J-200D spectropolarimeter with a liquid $N_2$-cooled InSb detector and equipped with an Oxford Instruments SM4000-7 tesla (T) superconducting magnet. CD measurements were taken at 5 °C in an anaerobic cuvette. CD spectra were corrected for buffer and protein baselines by subtraction, and MCD spectra were corrected for the natural CD and zero-field baseline effects by averaging the positive and negative field data at a given temperature.

## RESULTS

*Kinetic Parameters and pH Profile of Wild-Type (WT) Dke1*. The steady state kinetic parameters of WT Dke1 at pH 7.5 toward a range of dicarbonyl substrates have been investigated previously (*17*, *18*, *25*).[4] To gain information about the ionizable groups involved in catalysis, $k_{cat}^{app}$ and $K_M^{app}$ values were determined using PD for WT Dke1 between pH 5 and 10. Figure 2A shows these values as a function of pH.

The $\log(k_{cat}^{app}/K_M^{app})$ versus pH plot showed a clear bell shape with inflections in the acidic and basic pH regions with slopes of +1 and −1. Data were fit to eq 2:

$$Y = \log[C/(1 + K_1/[H^+] + [H^+]/K_2)] \quad (2)$$

where $Y$ is $\log(k_{cat}^{app})$ or $\log(k_{cat}^{app}/K_M^{app})$, $C$ is the pH-independent value of $Y$, and $K_1$ and $K_2$ are the macroscopic dissociation constants for the ionizable groups being titrated. $[H^+]$ is the proton concentration. From this fit, p$K_a$ values of 6.3 ± 0.4 and 8.4 ± 0.4 were determined. Given that $k_{cat}^{app}$ mirrors the $O_2$ reduction rate, which is the first step of the chemical reaction (*18*), this indicates that some precatalytic step is influenced by either enzyme or substrate ionization and is therefore pH-dependent. It should be noted that the substrate, PD, has a p$K_a$ of 8.9 and is considered to bind as a monoanion to the metal center (*18*, *26*). As a result, a change in its protonation state may well affect substrate affinity and substrate binding rates.

The $k_{cat}^{app}$ values are constant over the pH range investigated, with only a slight decrease in the $k_{cat}^{app}$ observed above pH 10 and below pH 5.5, where protein instability began to interfere with activity measurements. Because of this protein instability, it was not possible to determine whether the slight curvature in the extremes of the plots reflects a protonation equilibrium. Data were fit by eq 2 (vide supra), and the resulting curve eliminated the possibility of a p$K_a$ in the range of pH 4.2−10.0 (Figure 2A).

To test if the protonation state of the substrate is affecting the enzyme kinetics, $k_{cat}/K_M^{app}$−pH profiles for Dke1 were determined using TPD, the trifluorinated substrate analogue of PD, which has a p$K_a$ of 6.6 (*18*, *26*), more than 2 log units lower than that of PD. The resulting $k_{cat}^{app}/K_M^{app}$−pH profile showed an inflection in the basic region with a p$K_a$ value of 8.1 ± 0.2 (Table 2 and Figure S2B of the Supporting Information), the same as that for PD within experimental error. Therefore, the basic p$K_a$ found

[4]It should be noted that Dke1 could not be saturated with $O_2$ up to a $c_{O_2}$ of 1.2 mM, preventing the determination of kinetic constants under saturating conditions.

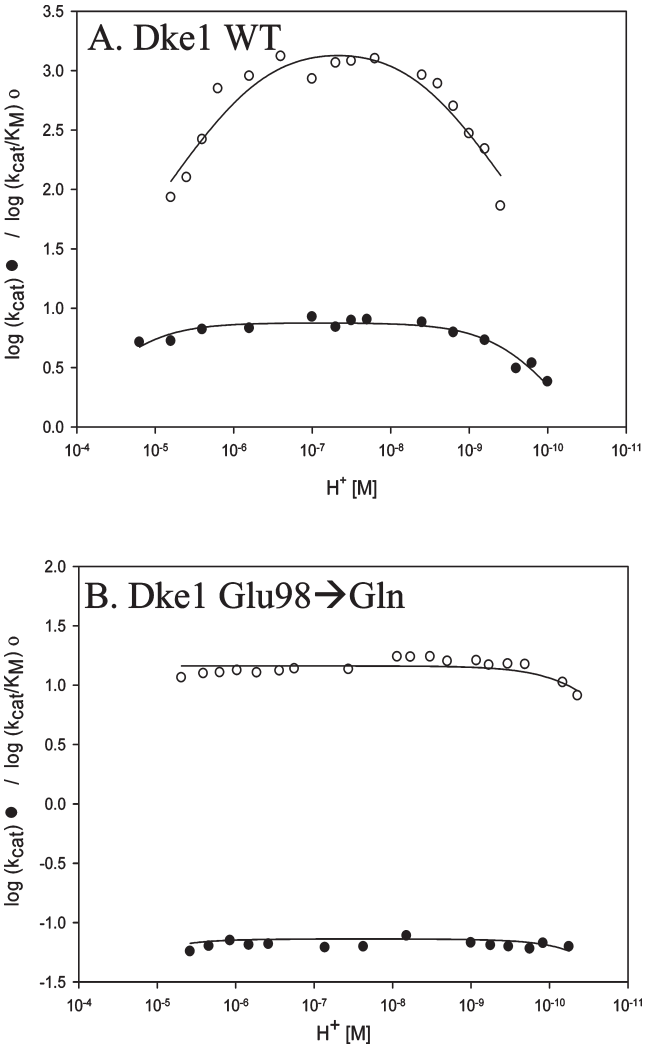


FIGURE 2: $k_{cat}^{app}/K_M^{app}$ and $k_{cat}^{app}$ profiles for (A) wild-type Dke1 and (B) the Glu98 → Gln variant, obtained at 25 °C in air-saturated buffer.

in the $k_{cat}^{app}/K_M^{app}$−pH profile was clearly not due to substrate deprotonation. At pH < 6.0, no reliable data could be obtained due to enzyme inactivation and slow reaction rates and a low extinction coefficient with TPD.

*Kinetic Parameters and pH Profiles of Second-Sphere Variants of Dke1*. (*i*) *Kinetic Parameters*. To gain insight into the role of H-bonding residues in dicarbonyl cleavage, hydrophilic amino acid residues with a potential role in catalysis were identified and subjected to mutagenesis. The structure of Dke1 reveals a mononuclear metallocenter, ligated by three histidines, His62, His64, and His104, in an active site pocket predominantly lined with hydrophobic residues and accessible via a hydrophobic tunnel (PDB entry 3bal). Only four hydrophilic amino acid residues are present in the substrate binding pocket. A hydrophilic gate formed by Arg80, Glu98, and Tyr70 connects the hydrophobic cavity with the exterior (Figure 1). The glutamate residue, Glu98, is a second-shell residue, positioned adjacent to the metal-ligating His104, with its proximal carboxylate O within H-bonding distance of the $\varepsilon^2$-NH group of the histidine (2.82 Å). Furthermore, Glu98 forms a salt bridge with Arg80. This structure H-bonds to a water molecule, which is further H-bonded to Tyr70, forming the hydrophilic gate. The fourth hydrophilic residue found in the active site is Thr107, which is situated in the outer coordination shell of $Fe^{2+}$. All four

Table 2: Steady State Kinetic Properties of WT Dke1 and Its Variants[a]

| | $k_{cat}^{app}$ ($s^{-1}$) | $K_M^{app}$ (mM $s^{-1}$) | $Fe^{2+}$ (%) | p$K_{a2}$ |
|---|---|---|---|---|
| WT | 6.6 | 9.1 ± 1.5 (*21*) | 70 | 8.4 ± 0.4 (8.1 ± 0.2)[b] |
| E98A | 0.074 | 4.1 ± 2 | 60 | −/ > 10 |
| E98Q | 0.050 | 2.9 ± 2 | 71 | −/ > 10 |
| R80A | 0.126 | 37 ± 15 | 50 | 9.0 ± 0.5 |
| Y70F | 1.27 | 8.5 ± 3 | 64 | 9.1 ± 0.5 |
| Y70A | 0.13 | 35 ± 15 | 51 | nd |
| T107A | 0.1 | nd[c] | 5 | nd |
| E98A/R80A | 0.098 | 35 ± 15 | 47 | nd |
| E98A/R80A/Y70F | 0.033 | nd[c] | 38 | nd |
| E98A/R80A/Y70A° | 0.007 | nd[c] | 68 | nd |

[a]Kinetic constants were determined in air-saturated buffer, at pH 7.5 and 25 °C. The typical iron content of an enzyme preparation ($Fe^{2+}$) is given, and p$K_{a2}$ values obtained for the "basic" inflection in the $k_{cat}^{app}/K_M^{app}$−pH correlation of WT and each variant are given. The $k_{cat}^{app}$ values shown are relative standard deviations of < 20%. The experimental error of all $Fe^{2+}$ contents was < 10% and corresponded to their total iron determined by ICP-MS (error of < 1%). [b]The p$K_a$ for the substrate TPD is given in parentheses. [c]No variation of catalytic rates at substrate concentrations of 400 and 600 $\mu$M was obtained; therefore, the resulting velocities were considered to mirror enzyme saturation and, therefore, $k_{cat}^{app}$.

residues were subjected to mutagenesis, and the resulting protein variants were characterized to elucidate their role in catalysis.

Variants were constructed, expressed, and purified where Tyr70, Arg80, Glu98, and Thr107 were individually and in combination substituted with alanine. Additionally, the "structurally conservative" mutants Tyr70 → Phe and Glu98 → Gln were produced. Iron contents were determined for all variants. Notably, for Thr107 → Ala, the iron content was < 5% in all preparations, and reconstitution of this enzyme variant with $Fe^{2+}$ could not be achieved, indicating a disruption of the metal binding site. All other variants showed iron contents of > 50% after purification, indicative of an intact metal binding site and allowing further characterization.

The steady state kinetic properties of all variants and typical $Fe^{2+}$ content are given in Table 2 and summarized below. The substitution of Glu98 with alanine showed a remarkable, ~100-fold reduction in $k_{cat}^{app}$ (0.074 $s^{-1}$). The analogous substitution with glutamine resulted in a similarly diminished reaction rate ($k_{cat}^{app}$ = 0.050 $s^{-1}$). A comparable decrease in $k_{cat}^{app}$ of 2 orders of magnitude was also found for the Arg80 → Ala variant ($k_{cat}$ = 0.126 $s^{-1}$). The substitution of Tyr70 with alanine resulted in a 60-fold decrease in $k_{cat}^{app}$, while the structurally conservative mutation to phenylalanine led to a minor, 3-fold decrease of the catalytic rate. No major changes were found for the $K_M^{app}$ values of the variants investigated. Thus, mutations perturbing the "hydrophilic gate", formed by Glu98, Arg80, and Tyr70, led to a reduction in $k_{cat}^{app}$ by 2 orders of magnitude. Dke1 variants bearing double and triple mutations were constructed to characterize the interplay of the particular mutations. Simultaneous substitution of Glu98 and Arg80 with alanine resulted in $k_{cat}^{app}$ values comparable to those of the respective single mutants. The additional exchange of Tyr70, thus completely abolishing the hydrophilic gate, had an additional diminishing effect on $k_{cat}^{app}$.

In a previous study on WT Dke1, it was determined that the reduction of $O_2$, which coincided with the enzyme−substrate complex decay rate ($k_{decay}^{app} = k[O_2]$), constituted the rate-limiting step of catalysis ($k_{cat}^{app}$). This rate was characterized by a strong dependence of $k_{cat}^{app}$ on the potential of the substrate to donate electrons which is mirrored by the energy level of its highest occupied molecular orbital ($\varepsilon_{HOMO}$) (*18*). Analogous correlations of $k_{decay}^{app}$ with the $\varepsilon_{HOMO}$ of the substrate, obtained for the variants described above, show that the nature of the rate-limiting step has not changed upon mutation (see Figure S1 of the Supporting Information).

(*ii*) *pH Profiles*. To investigate the apparent role of ionizable groups in the precatalytic steps of reactivity in Dke1, pH profiles of the steady state kinetic parameters for the variants Glu98 → Ala, Arg80 → Ala, and Tyr70 → Phe were determined. Importantly, the $k_{cat}^{app}/K_M^{app}$−pH profiles of the Glu98 → Ala and Glu98 → Gln variants of Dke1 showed an apparent elimination of both the acidic and basic p$K_a$ effects (Figure 2B and Figure S2A of Supporting Information)[5]Alternatively, for the variants Arg80 → Ala and Tyr70 → Phe, the basic p$K_a$ values were conserved, demonstrating that these residues are not associated with the basic $k_{cat}^{app}/K_M^{app}$−pH curve inflection (Figure S2C,D of the Supporting Information). As in WT Dke1, the $k_{cat}^{app}$ rates were not pH-dependent in all cases, over the entire pH range investigated. Results from $k_{cat}^{app}/K_M^{app}$−pH profiles are summarized in Table 2. The $k_{cat}^{app}/K_M^{app}$−pH profiles and $k_{cat}^{app}$−pH profiles for all variants are given in the Supporting Information.

*Stopped-Flow Kinetic Analysis of Substrate Binding*. To further define the pH dependence of the precatalytic steps and, in particular, the apparent elimination of the pH dependence of the $k_{cat}^{app}/K_M^{app}$−pH profiles for the Glu98 variants, the substrate net binding rates of WT Dke1 and variants were determined by stopped-flow kinetic measurements. Ligation of substrate to the metal center was monitored by measuring the formation of an absorption band which evolves upon ligation of a diketonate to the $Fe^{2+}$ cofactor and has been suggested previously to result from a MLCT transition (*18*).

Substrate binding was assessed using PD and DPD as ligands. The latter substrate binds more slowly than PD and allows for the initial, fast binding phase to be monitored (*18*). Variation of ligand concentration (0.15−5 mM) did not lead to a change in the binding rate under the conditions used (inset, Figure 3A), which implies that ligation of the diketonate to the metal cofactor was assessed under saturating conditions, and substrate ligation is not the first kinetic step of substrate binding. This is in line with a scenario in which the rates observed mirror the net rate of exchange of water and substrate ligands at the $Fe^{2+}$ center and not prebinding steps.

Rates of binding of DPD to variants Glu98 → Gln, Glu98 → Ala, Tyr70 → Phe, and Arg80 → Ala were measured at pH 7.5 (Figure 3A and Table 3). Generally, curves were best fit with a

[5]Protein instability precludes measurements of the $k_{cat}^{app}/K_M^{app}$ above pH 10. The curvature in the $k_{cat}^{app}/K_M^{app}$−pH profile at high pH cannot be fit with eq 2, ruling out a p$K_a$ of < 10.

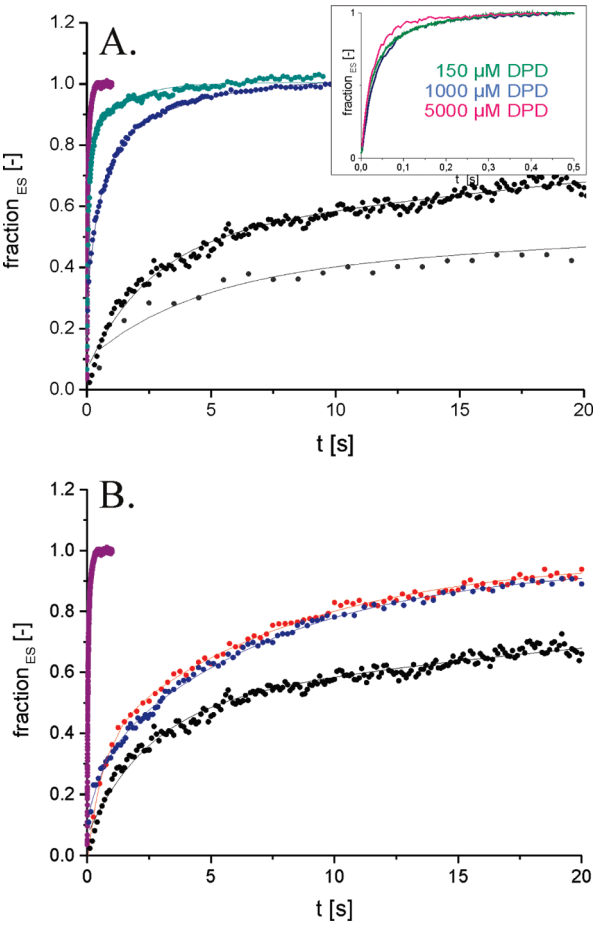


FIGURE 3: Stopped-flow traces of the Dke1 metallocenter with 1,1-difluoro-2,4-pentanedione (DPD). Traces were averaged from triplicate measurements. Panel A shows substrate binding rates for WT Dke1 (violet) and the outer sphere variants Tyr70Phe (blue), Arg80Ala (teal), Glu98Ala (dark gray), and Glu98Gln (black). The inset shows ligation of substrate to the $Fe^{2+}$ center at varying DPD concentrations. Panel B shows the pH dependence of substrate binding to WT Dke1 and the E98Q variant: traces for WT Dke1 at pH 7.5 (violet) and pH 9.5 (red) and traces for the Glu98 → Gln variant at pH 7.5 (black) and pH 9.5 (blue). Analogous rates for binding of two to four pentanediones are presented in the Supporting Information.

double-exponential decay, indicating a biphasic binding event. In the E98Q and E98A variants, the binding velocity is decreased by 2 ($k_1$) and 3 ($k_{1'}$) orders of magnitude, respectively. The Tyr70 → Ala and Arg80 → Ala substitutions caused an only moderate, 10-fold, reduction in binding rates. Binding curves with PD as a ligand showed the same general trend as those found for DPD (see Figure S3A of the Supporting Information), where, with the exception of the Glu98 variants, the initial binding phase was too fast to be assessed. Results are summarized in Table 3.

To further investigate the elimination of the basic p$K_a$ effect on the $k_{cat}^{app}/K_M^{app}$–pH profile upon Glu98 substitution, the binding kinetics for WT Dke1 and the Glu98 → Gln variant were determined at varying pH values. Measurements were performed at pH 7.5 and 9.5, which are approximately 1 log unit below and 1 log unit above the p$K_a$ of 8.4, respectively, determined from the $k_{cat}^{app}/K_M^{app}$–pH profile of WT Dke1 (vide supra). The resulting curves obtained for DPD ligation are shown in Figure 3B, and the associated rate constants are given in Table 3. The low- and high-pH forms of the Glu98 → Gln variant clearly show different binding characteristics, with the low-pH form showing a biphasic binding behavior with a pronounced

Table 3: Kinetic First-Order Rate Constants of Substrate Ligation for WT Dke1 and Variants from Stopped-Flow Kinetic Studies[a]

| | substrate | pH | $k_1$ ($s^{-1}$) | $k_{1'}$ ($s^{-1}$) |
|---|---|---|---|---|
| WT | PD | 7.5 | > 2000 | 180 |
| WT | DPD | 7.5 | 55 | 10 |
| E98Q | PD | 7.5 | 1.3 | 0.15 |
| E98Q | DPD | 7.5 | 0.28 | 0.02 |
| E98A | DPD | 7.5 | 0.23 | 0.008 |
| R80A | PD | 7.5 | 56 | – |
| R80A | DPD | 7.5 | 13.5 | 0.75 |
| Y70F | PD | 7.5 | 7.15 | – |
| Y70F | DPD | 7.5 | 1.9 | 0.30 |
| WT | PD | 9.5 | 330 | 25 |
| WT | DPD | 9.5 | 1.6 | 0.13 |
| E98Q | PD | 9.5 | 1.7 | 0.12 |
| E98Q | DPD | 9.5 | 0.3 | – |

[a]Data were obtained at 25 °C and at air saturation. The experimental error for all rate constants is > 20%.

slower phase compared to the apparently monophasic high-pH form.

In WT Dke1, the analogous shift resulted in ~30-fold ($k_1$) and ~80-fold ($k_{1'}$) decreases in binding rates. PD binding curves, again, showed the same trend that was found for DPD (see Figure S3B of the Supporting Information); however, fast substrate ligation rates and a probable change in the substrate protonation state in the pH range investigated influence the substrate binding rates and complicate the data analysis. The sensitivity and robustness of substrate binding velocities of WT Dke1 and the Glu98 variants, respectively, to a pH shift from 7.5 to 9.5 mirror their $k_{cat}^{app}/K_M^{app}$–pH profile characteristics.

Taken together, the results from stopped-flow kinetics show that Glu98 promotes substrate ligation when the pH is less than the p$K_a$ of 8.4. Given that a p$K_a$ of 8.4 is extraordinarily high to be associated with glutamic acid ionization and when the fact that there is no other ionizable group in the active site is considered, one explanation for this effect is a possible role of metal-bound water in the basic p$K_a$ process. (Note that $Fe^{2+}$-bound water usually shows a p$K_a$ of ~9, depending on the environment.) A combination of near-infrared (NIR) CD and MCD was employed to directly probe the coordination at the $Fe^{2+}$ site as a function of pH in WT Dke1 and its E98Q variant.

*NIR-CD and MCD Spectroscopy of the Metal Center in WT Dke1 and Its Glu98Gln Variant*. CD and MCD are spectroscopic techniques that provide information about the coordination environment and ligand field at a metal cofactor site (*27*, *28*). In this way, these techniques can report changes at the active site complementary to the kinetic results. We studied WT Dke1 and the E98Q variant via CD and MCD spectroscopy to explore the pH dependence observed in the kinetic measurements. (pD values are used here as the data must be obtained in $D_2O$.) A detailed description of the effects of the three-His ligand set on the $Fe^{2+}$ center in Dke1 relative to the two-His, one-carboxylate facial triad is forthcoming (*15*) and will not be covered here.

(*i*) *WT Dke1*. CD spectra of WT Dke1 were recorded between pD 7.0 and 9.5. The CD spectrum at pD 7.0 shows two transitions, one at 8000 $cm^{-1}$ (positive feature) and one at 10500 $cm^{-1}$ (negative feature). With an increase in pD, the spectrum shifts to one dominant positive peak at ~11000 $cm^{-1}$ (Figure 4A and Figure S4A of the Supporting Information). A plot of $\Delta\varepsilon$ versus pD for the transition at 11300 $cm^{-1}$ fits to a titration curve with a p$K_a$ of 8.2 ± 0.2 (Figure 4A, inset).

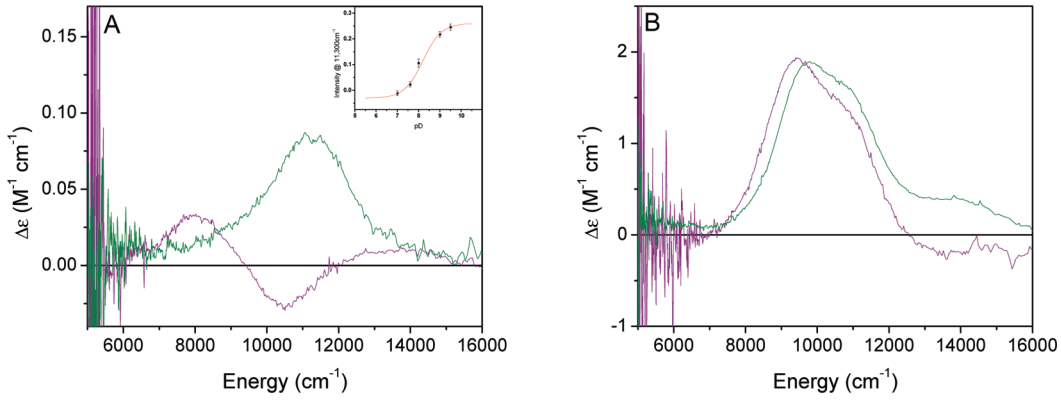


FIGURE 4: CD and LT MCD data for WT Dke1. (A) CD for pD 7.0 (purple) and pD 9.5 (green). The inset gives the intensity at 11300 cm$^{-1}$ as a function of pD. (B) LT MCD at 5 K and 7 T for pD 7.0 (purple, $\Delta\varepsilon \times 1.5$) and pD 9.5 (green).

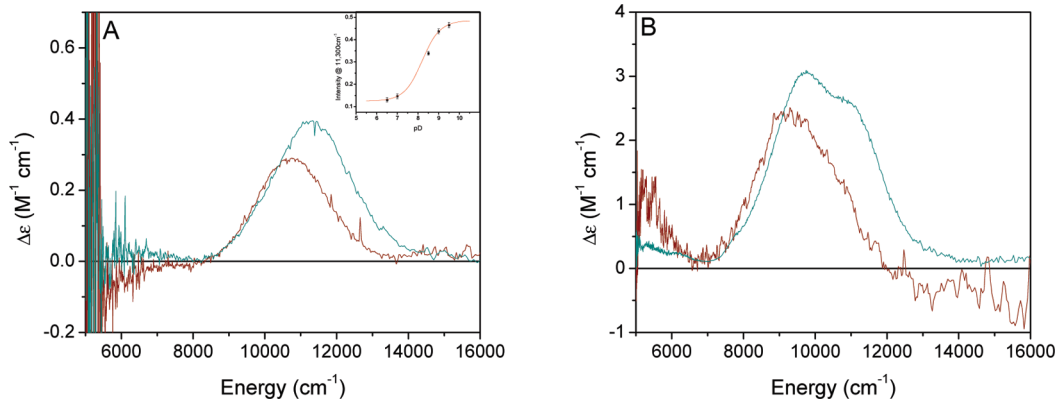


FIGURE 5: CD and LT MCD data for E98Q Dke1. (A) CD for pD 7.0 (red, $\Delta\varepsilon \times 4$) and pD 9.5 (teal). The inset gives the intensity at 11300 cm$^{-1}$ as a function of pD. (B) LT MCD at 5 K and 7 T for pD 7.0 (red) and pD 9.5 (teal).

To investigate whether the signals observed in CD were due to a change in the ligand field at the iron center or to a conformational change in the protein, we recorded low-temperature MCD spectra of the pD 7.0 and 9.5 samples. At pD 7.0, two positive transitions are observed centered at ~10100 cm$^{-1}$ and split by ~1900 cm$^{-1}$, which is characteristic of a 6C site. [From extensive studies on structurally defined $Fe^{2+}$ model complexes, 6C $Fe^{2+}$ exhibits two transitions in the ~10000 cm$^{-1}$ region, split by ~2000 cm$^{-1}$, 5C $Fe^{2+}$ shows one transition at ~10000 cm$^{-1}$ and one at ~5000 cm$^{-1}$, and 4C $Fe^{2+}$ shows transitions only in the 5000−7000 cm$^{-1}$ region (*27*, *28*).] When the pD is increased to 9.5, a very similar two-transition pattern is observed; however, the transitions are shifted up in energy by ~300 cm$^{-1}$ compared to those at pD 7.0 (Figure 4B).

(*ii*) *Dke1 Glu98 → Gln Variant*. To further explore the apparent effect of Glu98 on the p$K_a$ of substrate binding, CD and MCD experiments were conducted in parallel to those described above for the wild-type enzyme. The CD spectra of the E98Q variant exhibit one main peak at ~11000 cm$^{-1}$ that shifts up in energy (to ~11300 cm$^{-1}$) and up in intensity with an increase in pD (Figure 5A and Figure S4B of the Supporting Information). The inset of Figure 5A shows a plot of this intensity versus pD for E98Q Dke1. These data can be fit to a pD equilibrium with a p$K_a$ of 8.2 ± 0.2. The low-temperature MCD spectrum of the E98Q variant at pD 7.0 shows a significant spectral change compared to that of the wild type. A low-energy feature at ~5000 cm$^{-1}$ is now observed, characteristic of the presence of a 5C $Fe^{2+}$ species. The more intense asymmetric peak centered at ~9700 cm$^{-1}$ suggests two overlapping contributions, and since a 5C component can contribute only two transitions in the NIR spectral region, the third peak indicates the additional presence of a 6C $Fe^{2+}$ component. When the pD is increased to 9.5 in the E98Q variant, the spectrum changes to two transitions centered at ~10400 cm$^{-1}$. The spectrum indicates that only a 6C $Fe^{2+}$ species is now present. Additionally, these transitions occur at the same energies as those observed for the WT enzyme at pD 9.5 (Figure S5 of the Supporting Information).

*Autoxidation Studies of the E98Q Variant*. To determine whether the change in the metal center geometry to a partial five-coordinate species had an impact on the autoxidation rate of the Glu98Gln variant, the $O_2$ consumption of the resting Glu98Gln variant was monitored at 25 °C. Notably, iron detachment rates (~0.0003 s$^{-1}$), estimated by the fereneS method (*23*), are 2−3 orders of magnitude faster than apparent autoxidation rates determined for WT Dke1 at air saturation (*18*). Therefore, free iron will be present in equilibrium throughout the enzymic autoxidation [$K_{d\text{-}Fe} = 5\,\mu$M for WT Dke1 (*16*)], and consequently, the specific rate of autoxidation ($k_{autoox}^{app}$) will be complex, representing the oxidation of both bound and unbound iron. For the E98Q variant, a biphasic trace for $O_2$ consumption was observed, with a fast decay of ~15 $\mu$M $O_2$ followed by a slow rate of $O_2$ consumption (Figure S6 of the Supporting Information). The first, fast, phase of $O_2$ consumption shows the typical oxidation rate of unbound $Fe^{2+}$ [$k_{Fe}$ = 0.016 mM$^{-1}$ s$^{-1}$ (Figure S7 of the Supporting Information)] which is generally expected to be present in Fe(II)-containing enzyme preparations in equilibrium. The second phase reflects the autoxidation of the E98Q variant and has a specific rate of autoxidation ($k_{autoox}^{app}$)

of $1.2 \times 10^{-6}$ $s^{-1}$ related to $Fe^{2+}$. This value compares well to the slightly higher rate of autoxidation in WT Dke1 ($k_{autoox}^{app} = 7.5 \times 10^{-6}$ $s^{-1}$) (*18*), showing that the apparent autoxidation rate in the Glu98Gln variant is not elevated compared to that of WT Dke1.

## DISCUSSION

The hydrophilic residues in the substrate binding pocket of Dke1 are crucial for enzyme function in terms of (i) cofactor stability, (ii) stabilization of the 6C geometry at the metal center, and (iii) promotion of the transition state for $O_2$ reduction.

*Effect of Second-Shell Residues on Cofactor Stability in Dke1*. Thr107 stabilizes $Fe^{2+}$ binding, and mutation leads to a loss of cofactor affinity and function. In the crystal structure of Dke1 (Figure 1), Thr107 is within H-bonding distance of putative metal-bound waters (note that first-shell water molecules are missing in the crystal structure), suggesting a stabilization of the water ligands. Destabilization of the metal center by 1 order of magnitude following mutation of a second-shell threonine has been reported previously for the three-His-ligated metallo center of $Zn^{2+}$-dependent carbonic anhydrase. In this case, the crystal structure of the variant showed subtle geometric changes in the water shell (*29*, *30*). In Dke1, for which a $K_d$ of 5 $\mu$M for $Fe^{2+}$ has been determined previously (*16*), a decrease in affinity by 1 order of magnitude will lead to elimination of the high-affinity metal binding site.

Alternatively, Glu98, which is also located in the second shell of the metal center and interacts with the $\varepsilon^2$nitrogen of His104 by a 2.86 Å H-bond, shows no stabilizing effect on the metal center. The Glu98 variants of Dke1 actually lead to a 4-fold decrease in $Fe^{2+}$ detachment rates from 0.002 to 0.0005 $s^{-1}$. Second-sphere carboxylate residues H-bonded to the noncoordinated nitrogen of a metal-ligated histidine have been reported to increase metal cofactor stability when the carboxylate acts as a strong H-acceptor (*31*, *32*). In Dke1, the H-bonding interaction of Glu98 with Arg80 (Figure 1) lowers the p$K_a$ of Glu98 and likely prevents a similar role for Glu98 here.

*Stabilization of the 6C $Fe^{2+}$ Center*. A detailed kinetic analysis of WT Dke1 revealed new insight into the precatalytic steps of diketonate cleavage. Taking into account the proposed mechanism of Dke1 (*18*), where the diketonate coordinates to the $Fe^{2+}$ cofactor and the substrate-ligated metal center reduces $O_2$ via an encounter complex, precatalytic steps mirror the event of substrate binding. The $k_{cat}^{app}/K_M^{app}$−pH profile shows a bell shape with inflections in the acidic (p$K_a$ = 6.3) and basic (p$K_a$ = 8.4) ranges, corresponding to a pH dependence of binding rates, as $k_{cat}^{app}$ values are insensitive to pH in the range investigated (Figure 2). Protein instability prevented a detailed characterization of the low-pH effect. The high p$K_a$ was characterized further by stopped-flow measurements and CD and MCD spectroscopy.

Transient substrate binding kinetics of the WT enzyme generally showed a > 30-fold decrease in the rate of substrate ligation to $Fe^{2+}$ at pH 9.5 compared to that at pH 7.5, which parallels the pH effect seen in the $k_{cat}^{app}/K_M^{app}$ profile. Note that substrate binding rates determined were independent of DPD concentration in the range of 0.15−5 mM, showing that ligation of the substrate to the metal center is not the first kinetic step of substrate binding. It is therefore reasonable to view the velocities determined as net rates of ligand binding to the metal center and independent of access to the site. A reduction in the rate of binding at high pH suggests a stronger ligand set at the $Fe^{2+}$ center. This is consistent with deprotonation of one of the water ligands at the $Fe^{2+}$ center. The CD pH titration, which directly probes the $Fe^{2+}$ center, revealed a p$K_a$ of 8.2 for WT Dke1. The shift of the ligand field in the MCD data to a higher energy (Figure 4B) indicates a change at the $Fe^{2+}$ center to a stronger ligand. These data support a coordinated water−hydroxide equilibrium in WT Dke1. Hydroxide will be displaced more slowly than water by the substrate ligand, leading to decreased binding rates.[6] This is mirrored by an increased $K_M^{app}$ value in the enzyme kinetics of Dke1 and, consequently, the inflection of the $k_{cat}^{app}/K_M^{app}$−pH profile. A water−hydroxide equilibrium in this pH range is not commonly found for mononuclear non-heme $Fe^{2+}$ sites and represents a significant difference between the three-His ligation to $Fe^{2+}$ in Dke1 and the facial triad $Fe^{2+}$ ligation seen for many other ferrous enzymes. This depressed p$K_a$ of bound water likely reflects the reduced level of donation from the third histidine ligand compared to the carboxylate found in the standard facial triad enzymes.

Investigation of the Glu98 → Gln variant by CD spectroscopy showed a pH-dependent signal change with a p$K_a$ at pD ~8.2, analogous to the that of the wild-type enzyme. In the MCD data of E98Q Dke1 at pD 7.0, a mixture of 5C and 6C species is present. The presence of this 5C $Fe^{2+}$ species indicates that there is a reduced affinity for $H_2O$ in the absence of the carboxylate. Previous work has suggested that a carboxylate hydrogen bond can stabilize water binding to an $Fe^{2+}$ site (*8*). The MCD data for the E98Q variant at high pH show a completely 6C site. Hydroxide binds more tightly than water to the $Fe^{2+}$ center, and increasing the pH results in deprotonation of the water ligand giving a hydroxide that stays bound because of its increased affinity for $Fe^{2+}$. Combined, these data strongly support the model in which the p$K_a$ reflects deprotonation of a metal-bound water ligand. Therefore, Glu98 plays a role, directly or indirectly, in the stability of the bound water.

In the $k_{cat}^{app}/K_M^{app}$−pH profile of E98Q, both of the p$K_a$ effects have been eliminated. The acidic p$K_a$ may mirror slowed binding due to the protonation of Glu98; however, protein instability prevented further exploration of this effect. Pre-steady state kinetic substrate binding studies of the Glu98 → Gln and Glu98 → Ala variants showed a marked, > 100-fold, decrease in net binding rates. As opposed to the wild-type enzyme, substrate ligation rates at pH 7.5 and 9.5 were in the same time regime (Figure 3B), with $k_1$ values of 0.30 ± 0.02 and 0.28 ± 0.03 $s^{-1}$, respectively, consistent with the pH profile results that substrate binding velocities show no marked pH dependence between pH 7.5 and 9.5. The MCD data for E98Q show that the water−hydroxide equilibrium observed in WT is still present in this variant. Thus, the elimination of the pH effect on the E98Q variant is not due to the direct elimination of a water−hydroxide equilibrium at the $Fe^{2+}$ active site but a more indirect effect of a protein structural change due to the mutation in the vicinity of the site.

*Effect of the Hydrophilic Gate*. Glu98, Arg80, and Tyr70 form a hydrophilic gate that allows small hydrophilic molecules like water and the metal ion cofactor to access the hydrophobic active site. Mutation of each residue to the smaller alanine

[6]Note that the MCD spectra show a complete conversion to the PD-ligated metal center at pD 7.0 (*14*). In the kinetics, extinction coefficients of the enzyme−substrate complex are not significantly changed at high pH or with DPD as a ligand. This indicates that despite a shift in net binding rates, at equilibrium, the level of ligation of substrate to the metal center is > 90%.

destroys this gate. $O_2$ reduction rates in these variants are diminished by 2 orders of magnitude, confirming their crucial role in catalysis. The $k_{cat}^{app}$ rates are insensitive to pH in the range investigated, showing that acid−base catalysis is not involved in the rate-limiting step of $O_2$ reduction. One role of the gate may be in providing an H-bond that stabilizes the developing negative charge on $O_2$ in the transition state of the rate-determining step of $O_2$ reduction, a scenario invoked for the early steps of the mechanism in $Mn^{2+}$-dependent catechol dioxygenase (*33*). Loss of this H-bond can cause a 100−1000-fold reduction in the rate (10−20 kJ/mol). In the crystal structure of Dke1, Glu98, Arg80, and Tyr70 are oriented such that they could position one water molecule to provide this H-bond. Alternatively, destruction of the gate will allow more water molecules to enter the active site, and this may interfere with $O_2$ reduction. Further studies will be required to characterize the impact of active site hydrophilicity on catalysis.

## ACKNOWLEDGMENT

We thank Eva-Maria Imp for technical assistance. ICP-MS analyses were performed at the Institute of Analytical Chemistry at TU Graz.

## SUPPORTING INFORMATION AVAILABLE

QSAR analysis of Dke1−$Fe^{2+}$−diketonate complex decay and the electronic substrate structure for WT and variant Dke1, $k_{cat}$−pH and $k_{cat}/K_m$−pH profiles for Dke1 and its variants, stopped-flow binding curves for binding of PD to WT Dke1 and its variants, CD spectra of WT Dke1 and the Glu98Gln variant at varying pD values, and overlay of the MCD spectra of WT and E98Q Dke1 at pD 9.5. This material is available free of charge via the Internet at http://pubs.acs.org.

## REFERENCES

1. Costas, M., Mehn, M. P., Jensen, M. P., and Que, L., Jr. (2004) Dioxygen activation at mononuclear nonheme iron active sites: Enzymes, models, and intermediates. *Chem. Rev. 104*, 939–986.
2. Hegg, E. L., and Que, L., Jr. (1997) The 2-His-1-carboxylate facial triad-an emerging structural motif in mononuclear non-heme iron(II) enzymes. *Eur. J. Biochem. 250*, 625–629.
3. Solomon, E. I., Brunold, T. C., Davis, M. I., Kemsley, J. N., Lee, S. K., Lehnert, N., Neese, F., Skulan, A. J., Yang, Y. S., and Zhou, J. (2000) Geometric and electronic structure/function correlations in non-heme iron enzymes. *Chem. Rev. 100*, 235–350.
4. Groce, S. L., and Lipscomb, J. D. (2005) Aromatic ring cleavage by homoprotocatechuate 2,3-dioxygenase: Role of His200 in the kinetics of interconversion of reaction cycle intermediates. *Biochemistry 44*, 7175–7188.
5. Mendel, S., Arndt, A., and Bugg, T. D. (2004) Acid-base catalysis in the extradiol catechol dioxygenase reaction mechanism: Site-directed mutagenesis of His-115 and His-179 in *Escherichia coli* 2,3-dihydroxyphenylpropionate 1,2-dioxygenase (MhpB). *Biochemistry 43*, 13390–13396.
6. Siegbahn, P. E., and Haeffner, F. (2004) Mechanism for catechol ring-cleavage by non-heme iron extradiol dioxygenases. *J. Am. Chem. Soc. 126*, 8919–8932.
7. Viggiani, A., Siani, L., Notomista, E., Birolo, L., Pucci, P., and Di Donato, A. (2004) The role of the conserved residues His-246, His-199, and Tyr-255 in the catalysis of catechol 2,3-dioxygenase from *Pseudomonas stutzeri OX1*. *J. Biol. Chem. 279*, 48630–48639.
8. Neidig, M. L., Brown, C. D., Light, K. M., Fujimori, D. G., Nolan, E. M., Price, J. C., Barr, E. W., Bollinger, J. M., Jr., Krebs, C., Walsh, C. T., and Solomon, E. I. (2007) CD and MCD of CytC3 and taurine dioxygenase: Role of the facial triad in α-KG-dependent oxygenases. *J. Am. Chem. Soc. 129*, 14224–14231.
9. Straganz, G. D., and Nidetzky, B. (2006) Variations of the 2-His-1-carboxylate theme in mononuclear non-heme Fe(II) oxygenases. *ChemBioChem 7*, 1536–1548.
10. Blasiak, L. C., Vaillancourt, F. H., Walsh, C. T., and Drennan, C. L. (2006) Crystal structure of the non-haem iron halogenase SyrB2 in syringomycin biosynthesis. *Nature 440*, 368–371.
11. Wong, C., Fujimori, D. G., Walsh, C. T., and Drennan, C. L. (2009) Structural analysis of an open active site conformation of nonheme iron halogenase CytC3. *J. Am. Chem. Soc. 131*, 4872–4879.
12. Gudrun, R. (2002) Stranzl, Strukturuntersuchungen an Enzymen im Kristall und in Loesung. Ph.D. Dissertation, Karl Franzens University, Graz, Austria, pp 1−113.
13. Straganz, G., Brecker, L., Weber, H. J., Steiner, W., and Ribbons, D. W. (2002) A novel β-diketone-cleaving enzyme from *Acinetobacter johnsonii*: Acetylacetone 2,3-oxygenase. *Biochem. Biophys. Res. Commun. 297*, 232–236.
14. Straganz, G. D., Glieder, A., Brecker, L., Ribbons, D. W., and Steiner, W. (2003) Acetylacetone-cleaving enzyme Dke1: A novel C-C-bond-cleaving enzyme from *Acinetobacter johnsonii*. *Biochem. J. 369*, 573–581.
15. Diebold, A. R., et al. Manuscript in preparation.
16. Leitgeb, S., Straganz, G. D., and Nidetzky, B. (2009) Biochemical characterization and mutational analysis of the mononuclear non-haem $Fe^{2+}$ site in Dke1, a cupin-type dioxygenase from *Acinetobacter johnsonii*. *Biochem. J. 418*, 403–411.
17. Straganz, G. D., Hofer, H., Steiner, W., and Nidetzky, B. (2004) Electronic substituent effects on the cleavage specificity of a non-heme Fe(II)-dependent β-diketone dioxygenase and their mechanistic implications. *J. Am. Chem. Soc. 126*, 12202–12203.
18. Straganz, G. D., and Nidetzky, B. (2005) Reaction coordinate analysis for β-diketone cleavage by the non-heme Fe(II)-dependent dioxygenase Dke1. *J. Am. Chem. Soc. 127*, 12306–12314.
19. Wang, W., and Malcolm, B. A. (1999) Two-stage PCR protocol allowing introduction of multiple mutations, deletions and insertions using QuikChange site-directed mutagenesis. *BioTechniques 26*, 680–682.
20. Straganz, G., Slavica, A., Hofer, H., Mandl, U., Steiner, W., and Nidetzky, B. (2005) Integrated approach for production of recombinant acetylacetone dioxygenase from *Acinetobacter johnsonii*. *Biocatal. Biotransform. 23*, 261–269.
21. Skerra, A., and Schmidt, T. G. (2000) Use of the Strep-Tag and streptavidin for detection and purification of recombinant proteins. *Methods Enzymol. 326*, 271–304.
22. Higgins, T. (1981) Novel chromogen for serum iron determinations. *Clin. Chem. 27*, 1619–1620.
23. Johnson-Winters, K., Purpero, V. M., Kavana, M., Nelson, T., and Moran, G. R. (2003) 4-(Hydroxyphenyl)pyruvate dioxygenase from *Streptomyces avermitilis*: The basis for ordered substrate addition. *Biochemistry 42*, 2072–2080.
24. Pace, C. N., Vajdos, F., Fee, L., Grimsley, G., and Gray, T. (1995) How to measure and predict the molar absorption coefficient of a protein. *Protein Sci. 11*, 2411–2423.
25. Edelhoch, H. (1967) Spectroscopic determination of tryptophan and tyrosine in proteins. *Biochemistry 6*, 1948–1954.
26. Calculated using Advanced Chemistry Development (ACD/Laboratories) version 8.14 for Solaris ( 1994−2007) ACD/Laboratories, Scifinder Scholar.
27. Solomon, E. I., Pavel, E. G., Loeb, K. E., and Campochiaro, C. (1995) Magnetic circular dichroism spectroscopy as a probe of the geometric and electronic structure of non-heme ferrous enzymes. *Coord. Chem. Rev.,* 369–460.
28. Pavel, E. G., Kitajima, N., and Solomon, E. I. (1998) Magnetic Circular Dichroism Spectroscopic Studies of Mononuclear Non-Heme Ferrous Model Complexes. Correlation of Excited- and Ground-State Electronic Structure with Geometry. *J. Am. Chem. Soc. 120*, 3949–3962.
29. DiTusa, C. A., McCall, K. A., Christensen, T., Mahapatro, M., Fierke, C. A., and Toone, E. J. (2001) Thermodynamics of metal ion binding. 2. Metal ion binding by carbonic anhydrase variants. *Biochemistry 40*, 5345–5351.
30. Lachenmann, M. J., Ladbury, J. E., Dong, J., Huang, K., Carey, P., and Weiss, M. A. (2004) Why zinc fingers prefer zinc: Ligand-field symmetry and the hidden thermodynamics of metal ion selectivity. *Biochemistry 43*, 13910–13925.
31. Dudev, T., Lin, Y. L., Dudev, M., and Lim, C. (2003) First-second shell interactions in metal binding sites in proteins: A PDB survey and DFT/CDM calculations. *J. Am. Chem. Soc. 125*, 3168–3180.
32. Frison, G., and Ohanessian, G. (2009) Metal-histidine-glutamate as a regulator of enzymatic cycles: A case study of carbonic anhydrase. *Phys. Chem. Chem. Phys. 11*, 374–383.
33. Whiting, A. K., Boldt, Y. R., Hendrich, M. P., Wackett, L. P., and Que, L., Jr. (1996) Manganese(II)-dependent extradiol-cleaving catechol dioxygenase from *Arthrobacter globiformis* CM-2. *Biochemistry 35*, 160–170.